

To obtain the complete dependence on  $m/T$ , we use Eq. (10.68). For each particle species, subject to the existence of the series representation of the integral, as addressed earlier, the result is

$$\frac{S}{N} = 4 \frac{\sum_{n=1}^{\infty} \frac{(u\lambda)^n}{n^4} \left( (nx)^2 K_2(nx) + \frac{1}{4} (nx)^3 K_1(nx) \right)}{\sum_{n=1}^{\infty} \frac{(u\lambda)^n}{n^3} (nx)^2 K_2(nx)} - \ln \lambda, \quad (10.86)$$

where  $x = m\beta$ .  $u = -1$  for fermions and  $u = 1$  otherwise. For the non-relativistic limit  $x > 1$ , one can use Eq. (10.46) in Eq. (10.86) to obtain

$$\frac{S}{N} = \frac{\sum_{n=1}^{\infty} \frac{(u\lambda)^n}{n^4} (nx)^2 K_2(nx) I(nx)}{\sum_{n=1}^{\infty} \frac{(u\lambda)^n}{n^3} (nx)^2 K_2(nx)} - \ln \lambda, \quad (10.87)$$

$$I(nx) = \frac{5}{2} + nx + \frac{15}{8} \frac{1}{nx} - \frac{15}{8} \frac{1}{(nx)^2} + \frac{135}{128} \frac{1}{(nx)^3} + \dots, \quad (10.88)$$

which, for  $n = 1$ , yields the result Eq. (10.82), once we rearrange terms of two components to include particles and antiparticles and divide by the baryon number (particle–antiparticle difference).

For the case of a vanishing chemical potential, the non-relativistic Boltzmann approximation, Eq. (10.80), is quite appropriate. In Fig. 10.5, we compare the entropy per particle, evaluated at zero chemical potential ( $\lambda = 1$ ), for the Fermi (long-dashed line), Bose (short-dashed line) and Boltzmann (solid line, see Fig. 10.4) particles.

## 11 Hadronic gas

### 11.1 Pressure and energy density in a hadronic resonance gas

We now consider the physical properties of a hadronic, confined phase, such as energy density, pressure, and abundances of various particles, assuming that we have a locally thermally and chemically equilibrated phase. Although full chemical equilibrium is most certainly not attainable in the short time of the nuclear-collision interaction, see chapter 5, this study provides very useful guidance and a reference point for understanding the properties of hadronic matter out of chemical equilibrium.

There are two ways to look at a hadronic gas: the first is that we can study its properties using the known hadronic states. This approach will

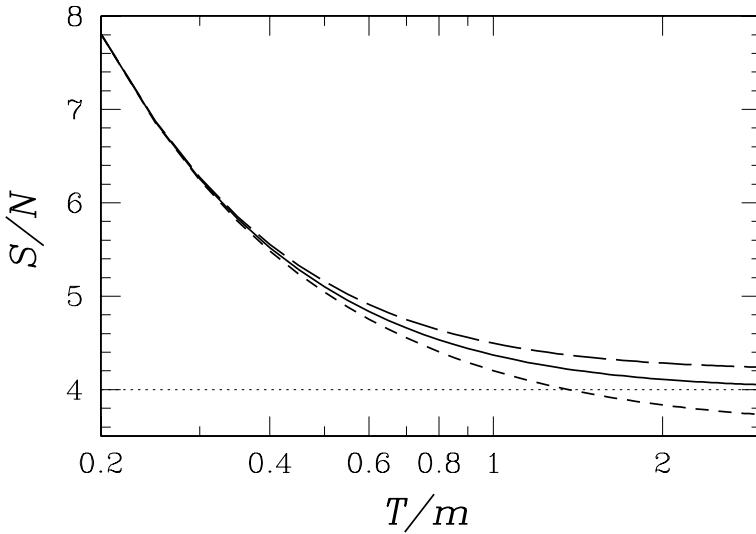


Fig. 10.5. Comparison of entropy per particle for Fermi and Bose gases, their classical Boltzmann limit, as a function of  $T/m$ : long-dashed Fermi gas, short-dashed Bose gas, solid line Boltzmann classical limit.

lead to difficulties when and if the temperature is high, since the contribution of high-mass resonances is apparently not convergent. Even though the population of each such state is suppressed exponentially by the Boltzmann factor  $e^{-m/T}$ , the number of states rises exponentially with mass, and compensates for this effect. This phenomenon was noticed almost 40 years ago. This led to the development of the statistical-bootstrap model (SBM) and the Hagedorn-gas model, which we will address in chapter 12.

In the physically most relevant hadron-gas domain,  $70 \text{ MeV} > T > 170 \text{ MeV}$ , each distinguishable hadron distribution is far from quantum degeneracy. Therefore, we can use the Boltzmann approximation. The only exceptional case is the pion, which, when necessary and appropriate, will be considered as a Bose particle. Each of the hadronic states is considered as a separate contributing fraction in the thermal and chemically equilibrated gas phase, with all fugacities set at  $\lambda = 1$  (no net quantum numbers, e.g.,  $b = 0$  etc.). The result is shown in Fig. 11.1. We included 4627 (counting spin and isospin degeneracy) hadronic states listed by the particle data group (PDG) [136]. No doubt many more hadronic resonances exist. However, as the mass of the new resonances increases, they become more difficult to characterize, given the dense background of the neighboring resonances, and normally increasing decay width, both of which effects are reducing the signal-to-noise ratio in the experiment.

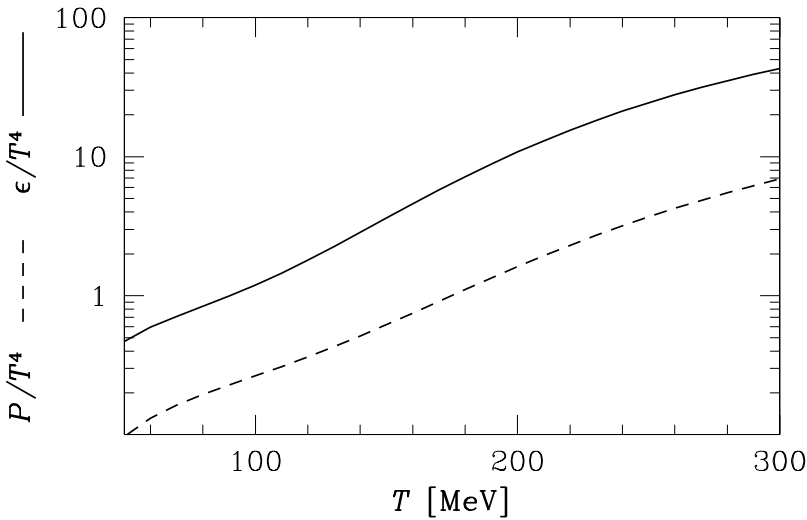


Fig. 11.1. The energy density (solid line) and pressure (dashed line) in units of  $T^4$  for all known hadrons (on a logarithmic scale) as functions of temperature  $T$ . All fugacities are set to unity.

The worrying fact is that the energy and pressure seem to grow well beyond the values spanned by the lattice calculations; see section 15.5. This happens since we have allowed very many hadrons to be present in the same volume. Even though each kind is relatively rare, the large number of resonances implies a considerable total particle density. However, hadrons are not point-like, and in some sense the presence of particles fills the space available. In the context of the statistical bootstrap, we will argue in section 12.3 that each hadron occupies a fraction of the spacial volume. This qualitative argument leads to a correction that relates the physically observable  $P$  and  $\epsilon$  to the point-particle result (subscript ‘pt’) we have so far studied [144]:

$$P = \frac{P_{\text{pt}}}{1 + \epsilon_{\text{pt}}/(4\mathcal{B})}, \quad \epsilon = \frac{\epsilon_{\text{pt}}}{1 + \epsilon_{\text{pt}}/(4\mathcal{B})}. \quad (11.1)$$

The energy density of a hadron is assumed to be  $4\mathcal{B}$ , where, as before,  $\mathcal{B}$  is the bag constant, and we recall the benchmark value,  $\mathcal{B}^{1/4} = 171$  MeV, corresponding to  $4\mathcal{B} = 0.45$  GeV fm $^{-3}$ . This excluded volume modifies and limits the growth both of  $\epsilon$  and of  $P$  with temperature. The magnitude of the effect depends on details of the implementation and on the parameters used. However,  $\epsilon/P$  is little influenced by this phenomenological uncertainty.

The dynamics of HG matter described in, e.g., the hydrodynamic approach in section 6.2 depends in a critical way on the ratio of the inertia

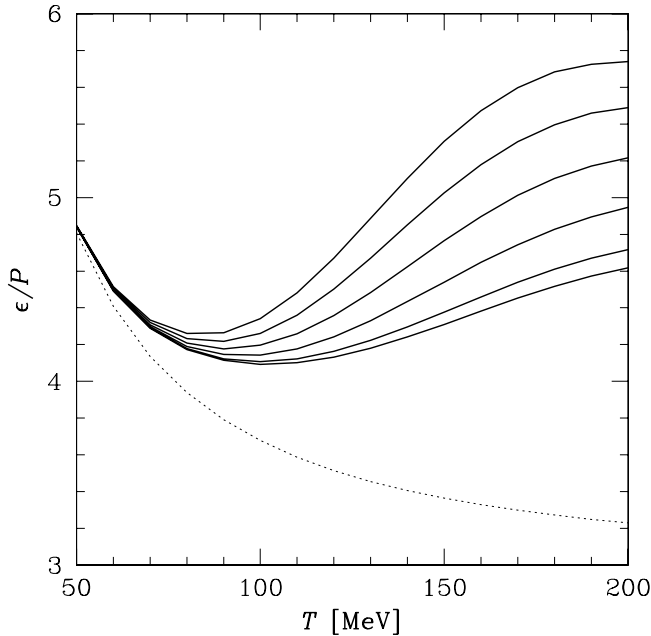


Fig. 11.2. The ratio of energy density and pressure for a hadronic gas as a function of the temperature  $T$ . Dotted line: pure pion gas; solid lines: gas comprising pions, nucleons, kaons, and  $\Delta(1232)$ , from bottom to top for  $\lambda_q = 1, 1.2, 1.4, 1.6, 1.8,$  and  $2$ .

(energy density) to force (pressure) . In Fig. 11.2 for several simple cases, we show the HG ratio  $\epsilon/P$ , as a function of temperature. The dotted curve is for the pure pion gas, and we see how the relativistic equation of state is approached for  $T > 100$  MeV. Remarkably, a very different result is seen once heavy hadrons are introduced. The solid lines include, apart from pions, a few more massive states: nucleons, kaons, and  $\Delta(1232)$ . The solid lines from bottom to top are for  $\lambda_q = 1, 1.2, 1.4, 1.6, 1.8,$  and  $2$ . We recognize that increasing  $\lambda_q$  (i.e. increasing the massive-baryon component) leads to a greater ratio of inertia to force. This result is clearly independent of the (schematic) finite-volume correction we introduced in Eq. (11.1). A fully realistic calculation of this situation is presented in Fig. 11.3, for the case  $\lambda_s = 1.1$  and  $\gamma_s/\gamma_q = 0.8$  for  $\lambda_q = 1$  to  $2$  in steps of  $0.2$  from bottom to top, and  $\gamma_q = 1$  (dashed lines), or  $\gamma_q = e^{m_\pi/(2T)}$  (full lines). Imagine that a hadron phase is formed from a deconfined QGP at some temperature  $T > 140$  MeV. In view of these results, we then expect an accelerating flow of matter as the ratio of inertia to force decreases, until a minimum is reached at  $T = 90$  MeV. At this point, the HG phase most likely ceased to exist, in the sense that the distance particles travel

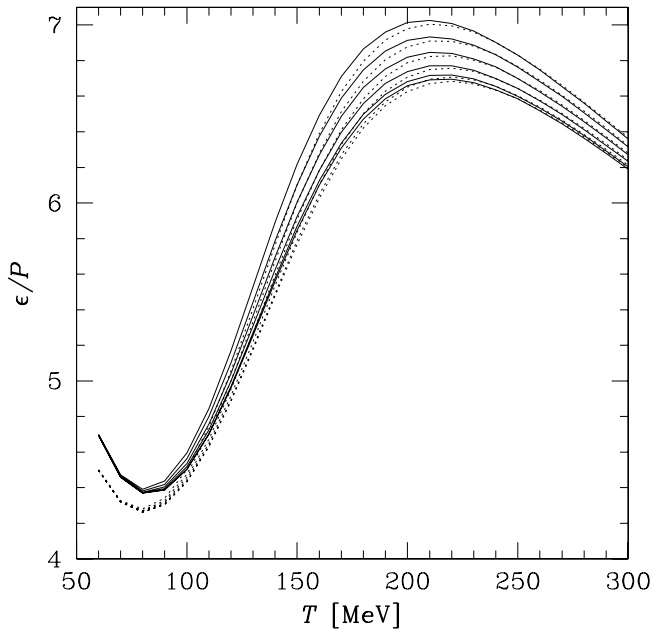


Fig. 11.3. The energy density over pressure for a hadronic gas with statistical parameters  $\lambda_s = 1.1$  and  $\gamma_s/\gamma_q = 0.8$ , with  $\lambda_q = 1$  to 2 in steps of 0.2 from bottom to top, and  $\gamma_q = 1$  (dashed lines), or  $\gamma_q = e^{m_\pi/(2T)}$  (full lines).

between scattering had become too large. At the time of writing this book, it is not clear whether the hadronic phase is present at all, since in the sudden breakup of a QGP a direct transition to free-streaming hadrons produced sequentially in time can be imagined. However, these results apply certainly to the case in which no QGP is formed, namely at sufficiently low collision energy.

## 11.2 Counting hadronic particles

There are several discrete quantum numbers of a hadron gas that are conserved and require introduction of independent chemical potentials. The chemical potentials for conservation of baryon number and strangeness,  $\mu_B$  and  $\mu_S$ , are the best known. Alternatively, and more conveniently for our purposes, one can use the quark chemical potentials  $\mu_q$  and  $\mu_s$  for light and strange quarks, respectively. We will often differentiate between the u and d quarks, and use  $\mu_u$  and  $\mu_d$ .

This choice of quark chemical potentials is a matter of convenience and is made in order to facilitate the translation of QGP-phase variables into HG-phase variables; in no way does it assume deconfinement of quarks.

The relationship between the two sets of chemical potentials, quark-based and traditional hadron-conserved-quantum-number based, is given by the natural relations

$$\mu_b = 3\mu_q, \quad \mu_b = 3T \ln \lambda_q, \quad (11.2a)$$

$$\mu_S = \mu_q - \mu_s, \quad \mu_s = \mu_b/3 - \mu_S, \quad (11.2b)$$

where the minus signs are due to the conventional assignment of strangeness  $-1$  to the strange quark. Expressed in term of the fugacities we have:

$$\lambda_b = \lambda_q^3, \quad \lambda_S = \lambda_q/\lambda_s. \quad (11.3)$$

$B_h$  and  $S_h$  are the baryon number and strangeness of hadron 'h', and its chemical potential can be written either in terms of  $\mu_b$  and  $\mu_S$ , or in terms of  $\mu_q$  and  $\mu_s$ :

$$\mu_h = B_h\mu_b + S_h\mu_S, \quad (11.4a)$$

$$\mu_h = \nu_h^q\mu_q + \nu_h^s\mu_s, \quad (11.4b)$$

where  $\nu_h^q$  and  $\nu_h^s$  count the numbers of light and strange valence quarks inside the hadron, respectively, with antiquarks counted with a minus sign. By adapting the quark-based chemical potentials for hadrons, we recognize the fact that, in the quark model, the quantum numbers of hadrons are obtained by adding the quantum numbers of their constituent quarks.

The particle numbers are more directly addressed in the partition function in terms of fugacities. Since the fugacities are obtained by exponentiating the chemical potentials, Eq.(4.18), the fugacity of each hadronic species is simply the product of the fugacities of the valence quarks. We view a hadron as simply a carrier of the valence quarks, which determine the fugacity and chemical potential of each particle. For example, we have

$$\begin{aligned} p: \quad \mu_p &= 2\mu_u + \mu_d, & \lambda_p &= \lambda_u^2\lambda_d; \\ n: \quad \mu_n &= \mu_u + 2\mu_d, & \lambda_n &= \lambda_u\lambda_d^2; \\ \Lambda: \quad \mu_\Lambda &= \mu_u + \mu_d + \mu_s, & \lambda_\Lambda &= \lambda_u\lambda_d\lambda_s; \quad \text{etc.} \end{aligned}$$

We distinguish between the up and down quarks by introducing separate chemical potentials  $\mu_u$  and  $\mu_d$ , which is tantamount to introduction of the chemical potential  $\mu_Q$  related to the conservation of electrical charge. In view of the quark baryon number  $\frac{1}{3}$  and the quark charges  $-\frac{1}{3}$  and  $+\frac{2}{3}$ , the relations between the chemical potentials are

$$\mu_u \equiv \frac{1}{3}\mu_b + \frac{2}{3}\mu_Q, \quad \mu_d \equiv \frac{1}{3}\mu_b - \frac{1}{3}\mu_Q. \quad (11.5)$$

The average of  $\mu_u$  and  $\mu_d$  is the quark chemical potential  $\mu_q$ :

$$\mu_q \equiv \frac{\mu_u + \mu_d}{2}. \tag{11.6}$$

The definitions Eqs. (11.5) and (11.6) imply a modification of Eq. (11.2a),

$$\mu_q \rightarrow \mu_q = \frac{1}{3}\mu_b + \frac{1}{6}\mu_Q, \tag{11.7}$$

which is rarely considered. It arises from the fact that a quark system containing (nearly) equal numbers of u and d quarks would still have a net (positive) charge of a sixth the total number of u and d quarks, arising from the electrical charge of the proton in the initial state formed by the colliding nuclei.

The asymmetry in the number of u and d quarks is best described by the quantity

$$\delta\mu = \mu_d - \mu_u = -\mu_Q, \tag{11.8}$$

where the negative sign in the last equality reminds us that the d quark has negative charge. Inverting Eq. (11.7), we obtain

$$\mu_b = 3\mu_q \left( 1 + \frac{1}{6} \frac{\delta\mu}{\mu_q} \right). \tag{11.9}$$

In a free-quark gas with  $\mu_q < \pi T$ , we have, in view of Eq. (10.75),

$$\mu_d \propto \langle d - \bar{d} \rangle, \quad \mu_u \propto \langle u - \bar{u} \rangle, \tag{11.10}$$

where the net number (number of quarks minus that of antiquarks) of light quarks enters. In a QGP, we find the remarkably simple relation [216]

$$\frac{1}{6} \frac{\delta\mu}{\mu_q} = \frac{1}{3} \frac{\mu_d - \mu_u}{\mu_d + \mu_u} = \frac{1}{3} \frac{\langle d - \bar{d} \rangle - \langle u - \bar{u} \rangle}{\langle d - \bar{d} \rangle + \langle u - \bar{u} \rangle} = \frac{n - p}{A}, \tag{11.11}$$

with  $A = n + p$ , and  $n$  and  $p$  are the neutron and proton contents of the matter which formed the QGP phase.

For the case of greatest asymmetry available, in Pb–Pb collisions, we have  $\delta\mu/(6\mu_q) = 0.21$ . In the HG phase a similarly sized effect for  $\delta\mu/(6\mu_q)$  to that in a QGP is found, considering this issue numerically; see figure 1 in [183]. Especially in studying yields of individual particles, the specific quark u and d content can play a noticeable role. To see this, let us compare the u and d fugacities:

$$\frac{\lambda_d}{\lambda_u} = e^{\delta\mu/T} = \lambda_q^{\delta\mu/\mu_q}. \tag{11.12}$$

For Pb–Pb interactions under baryon-rich conditions, a  $\lambda_d/\lambda_u$  ratio significantly different from unity results. Some dilution of this phenomenon

will occur if a QGP is formed due to the contribution of hadronizing gluons, which do not differentiate between the two light  $u$  and  $d$  flavor states. We conclude that the  $u$ - $d$  asymmetry can not be completely ignored when one is considering the abundances of hadronic particles in baryon-rich fireballs.

Flavor-changing weak interactions are too slow to matter on the time scale of heavy-ion collisions. The strong and electro-magnetic interactions do not mix the quark flavors  $u$ ,  $d$ , and  $s$ . These are separately conserved on the time scale of hadronic collisions. Only the number of quark-antiquark pairs of the same flavor changes; that is, pairs can be produced or annihilated. The fugacities we call  $\gamma_q$  and  $\gamma_s$  serve to count the number of pairs of light and strange quark, respectively, at any given time. In general, these pair-abundance fugacities are rapidly evolving in time, in contrast to the fugacities  $\lambda_q$  and  $\lambda_s$ . In fact, for entropy-conserving evolution of a fireball of QGP, the fugacity  $\lambda_q$  is nearly constant, and, as we now shall address, as long as local conservation of strangeness is maintained,  $\lambda_s \simeq 1$ .

Comparing the QGP with the HG phase, the value of the strangeness fugacity  $\lambda_s$  is in a subtle and important way different. Given the mobility of individual quarks in the QGP phase, and ignoring the influence of electrical charge in this qualitative discussion, the phase space of both  $s$  and  $\bar{s}$  quarks must be the same, irrespective of the baryon content. To balance the  $s$  and  $\bar{s}$  distributions, we have  $\lambda_s = 1$ , irrespective of the value of  $\lambda_q$ , see, e.g., Eq.(4.42). It is instructive to check the phase-space integral describing the density of strangeness in order to appreciate these remarks, and to recall the precise physical difference between the fugacities  $\lambda_s$  and  $\gamma_s$ :

$$\langle n_s \rangle - \langle n_{\bar{s}} \rangle = \int \frac{d^3p}{(2\pi)^3} \left( \frac{1}{\gamma_s^{-1} \lambda_s^{-1} \exp\left(\frac{\sqrt{p^2+m_s^2}}{T}\right) + 1} - \frac{1}{\gamma_s^{-1} \lambda_s \exp\left(\frac{\sqrt{p^2+m_s^2}}{T}\right) + 1} \right). \quad (11.13)$$

We note the change in the power of  $\lambda_s$  between these two terms, and recognize that this integral can vanish only for  $\lambda_s \rightarrow 1$ . We discuss in the following section the small but significant asymmetry in  $\lambda_s$  due to the Coulomb charge present in baryon-rich quark matter: long-range electro-magnetic interactions influence strange and antistrange particles differently, and a slight deviation  $\lambda_s > 1$  is needed in order to compensate for this effect in the QGP phase.

Now, let us look at the HG phase. Strange quarks are bound in states comprising also light quarks. The presence of a net baryon number assures that there is an asymmetry in abundance of light quarks and antiquarks, and thus also, e.g., of strange baryons and antibaryons, with more hyperons than antihyperons being present. Owing to this asymmetry, strangeness cannot be balanced in the HG with the value  $\lambda_s = 1$ , unless the baryon density vanishes locally. We will address this important issue in a more quantitative manner in section 11.4. We have learned that a determination of  $\lambda_s = 1$  in the hadron-abundance analysis is indicating production of these hadrons directly in a breakup of a QGP phase, since a value different from unity is expected when a HG phase breaks up.

### 11.3 Distortion by the Coulomb force

It has been recognized for a long time that the Coulomb force can be of considerable importance in the study of relativistic heavy-ion collisions. It plays an important role in the HBT interferometry method of analysis of the structure of the particle source [57, 209]; section 9.3. The analysis of chemical properties is also subject to this perturbing force, and in consideration of the precision reached experimentally in the study of particle ratios, one has to keep this effect in mind.

We consider a Fermi gas of strange and antistrange quarks allowing that the Coulomb potential  $V_C$  is established by the excess charge of the colliding nuclei. Within a relativistic Thomas–Fermi phase-space occupancy model [193], and for finite temperature in a QGP, we have as generalization of Eq. (11.13) [177]

$$\langle N_s \rangle - \langle N_{\bar{s}} \rangle = \int_{R_f} g_s \frac{d^3r d^3p}{(2\pi)^3} \left( \frac{1}{1 + \gamma_s^{-1} \lambda_s^{-1} e^{(E(p) - \frac{1}{3} V_C(r))/T}} - \frac{1}{1 + \gamma_s^{-1} \lambda_s e^{(E(p) + \frac{1}{3} V_C(r))/T}} \right), \quad (11.14)$$

which clearly cannot vanish for  $V_C \neq 0$ , in the limit  $\lambda_s \rightarrow 1$ .

In Eq. (11.14), the subscript  $R_f$  on the spatial integral reminds us that only the classically allowed region within the fireball is covered in the integration over the level density;  $E = \sqrt{m^2 + \vec{p}^2}$ , and, for a uniform charge distribution within a radius  $R_f$  of charge  $Z_f$ ,

$$V_C = \begin{cases} -\frac{3 Z_f e^2}{2 R_f} \left[ 1 - \frac{1}{3} \left( \frac{r}{R_f} \right)^2 \right], & \text{for } r < R_f; \\ -\frac{Z_f e^2}{r}, & \text{for } r > R_f. \end{cases} \quad (11.15)$$

One obtains a rather precise result, for the range of parameters of interest to us, using the Boltzmann approximation:

$$\langle N_s^B \rangle - \langle N_{\bar{s}}^B \rangle = \gamma_s \left( \int g_s \frac{d^3 p}{(2\pi)^3} e^{-E/T} \right) \times \int_{R_f} d^3 r \left( \lambda_s e^{V_C/3T} - \lambda_s^{-1} e^{-V_C/3T} \right). \quad (11.16)$$

The Boltzmann limit allows us also to verify and confirm the signs: the Coulomb potential is negative for the negatively charged  $s$  quarks with charge  $\frac{1}{3}$ , which is made explicit in the potential terms in all expressions above. We have

$$\tilde{\lambda}_s \equiv \lambda_s \ell_C^{1/3} = 1, \quad \ell_C \equiv \frac{\int_{R_f} d^3 r e^{V/T}}{\int_{R_f} d^3 r}. \quad (11.17)$$

$\ell_C < 1$  expresses the Coulomb deformation of strange quark phase space.  $\ell_C$  is not a fugacity that can be adjusted to satisfy a chemical condition, since consideration of  $\lambda_i$ ,  $i = u, d, s$ , exhausts all available chemical balance conditions for the abundances of hadronic particles, and allows introduction of the fugacity associated with the Coulomb charge of quarks and hadrons; see section 11.2. Instead,  $\ell_C$  characterizes the distortion of the phase space by the long-range Coulomb interaction. This Coulomb distortion of the quark phase space is naturally also present for  $u$  and  $d$  quarks, but appears less significant given that  $\lambda_u$  and  $\lambda_q$  are empirically determined. On the other hand this effect compensates in part the  $u$ - $d$  abundance asymmetry effect we have discussed in Eqs. (11.5)–(11.12).

Choosing  $T = 140$  MeV and  $m_s = 200$  MeV, and noting that the value of  $\gamma_s$  is practically irrelevant since this factor cancels out in the Boltzmann approximation, see Eq. (11.16), we find for  $Z_f = 150$  that the value  $\lambda_s = 1.10$  is needed for  $R_f = 7.9$  fm in order to balance the Coulomb distortion. One should remember that the dimensionless quantities  $m_s/T$  and  $R_f T$  determine the magnitude of the effect we study. Chemical freeze-out at higher temperature, e.g.,  $T = 170$  MeV, leads for  $\lambda_s = 1.10$  to somewhat smaller radii, which is consistent with the higher temperature used.

The influence of the Coulomb force on chemical freeze-out is relevant in central Pb–Pb interactions, whereas for S–Au/W/Pb reactions, a similar analysis leads to a value  $\lambda_s = 1.01$ , which is little different from the value  $\lambda_s = 1$  expected in the absence of the Coulomb deformation of phase space. Another way to understand the varying importance of the Coulomb effect is to note that, while the Coulomb potential acquires in the Pb–Pb case a magnitude comparable to the quark chemical potential, it remains small on this scale for S–Au/W/Pb reactions.

### 11.4 Strangeness in hadronic gas

We now describe the abundance of strange particles in the hadronic-gas phase. This is, compared with the QGP, a very complicated case, since there are many particles which are carriers of ‘open’ strangeness. Moreover, strong interactions result in the presence of numerous hadronic resonances with open strangeness. The postulate of the dominance by hadron resonance formation of hadron–hadron interactions [140] allows a vast simplification of the theoretical treatment. Regarding the hadronic-gas phase as a mixture of various non-interacting hadronic-resonance gases, all information about the interaction is contained in the mass spectrum  $\tau(m^2, b)$  which describes the number of hadrons of baryon number  $b$  in a mass interval  $dm^2$ . We will address this postulate in more detail in chapter 12. Within this approach to strong interactions, the logarithm of the total partition function is additive in its strange and not strange sectors, so long as the various gas fractions interact mainly via formation of hadronic resonances. We then have

$$\ln Z = \ln Z^{\text{non-strange}} + \ln Z^{\text{strange}}. \quad (11.18)$$

In the grand-canonical description, one finds that the non-strange hadrons influence the strange ones by providing a background value of statistical parameters, such as the baryochemical potential  $\mu_b$ , which are accessible to direct measurement. We conclude that, in order to understand abundances of strange particles, it is sufficient to consider  $\ln Z^{\text{strange}}$ . In the Boltzmann approximation, it is easy to write down the partition function for the strange-particle fraction of the hadronic gas,  $\mathcal{Z}_s$ . Including the possibility of an only partially saturated strange phase space through the factor  $\gamma_s$ , and similarly  $\gamma_q$  for light quarks, but suppressing for simplicity the isospin asymmetry  $\delta\mu$ , Eq. (11.8), we have

$$\begin{aligned} \ln \mathcal{Z}_s^{\text{HG}} = \frac{VT^3}{2\pi^2} & \left[ (\lambda_s \lambda_q^{-1} + \lambda_s^{-1} \lambda_q) \gamma_s \gamma_q F_K + (\lambda_s \lambda_q^2 + \lambda_s^{-1} \lambda_q^{-2}) \gamma_s \gamma_q^2 F_Y \right. \\ & \left. + (\lambda_s^2 \lambda_q + \lambda_s^{-2} \lambda_q^{-1}) \gamma_s^2 \gamma_q F_\Xi + (\lambda_s^3 + \lambda_s^{-3}) \gamma_s^3 F_\Omega \right]. \quad (11.19) \end{aligned}$$

In the phase-space function  $F_i$  all kaon (K), hyperon (Y), cascade ( $\Xi$ ), and omega ( $\Omega$ ) resonances plus their antiparticles are taken into account:

$$\begin{aligned} F_K &= \sum_j g_{K_j} W(m_{K_j}/T); \quad K_j = K, K^*, K_2^*, \dots, \quad m \leq 1780 \text{ MeV}, \\ F_Y &= \sum_j g_{Y_j} W(m_{Y_j}/T); \quad Y_j = \Lambda, \Sigma, \Sigma(1385), \dots, \quad m \leq 1940 \text{ MeV}, \\ F_\Xi &= \sum_j g_{\Xi_j} W(m_{\Xi_j}/T); \quad \Xi_j = \Xi, \Xi(1530), \dots, \quad m \leq 1950 \text{ MeV}, \end{aligned}$$

$$F_\Omega = \sum_j g_{\Omega_j} W(m_{\Omega_j}/T); \quad \Omega_j = \Omega, \Omega(2250). \quad (11.20)$$

The  $g_i$  are the spin–isospin degeneracy factors,  $W(x) = x^2 K_2(x)$ , see Eq. (10.50a) and Fig. 10.1, where  $K_2$  is the modified Bessel function, Eq. (10.44).

We need to understand, in terms of experimental observables, the chemical properties of the fireball at the time of hadron production. The method of choice is the study of particle ratios [167, 216]; section 9.1. In order to obtain the mean abundances of various strange particles, we introduce for each species its own dummy fugacity (which we subsequently will set equal to unity). The explicit expressions for these ratios turn out to be very simple, and one quickly deduces from the following examples the principles which allow one to construct any ratio:

$$\frac{\langle n_{\bar{\Lambda}} \rangle}{\langle n_{\Lambda} \rangle} = \lambda_q^{-4} \lambda_s^{-2}; \quad (11.21a)$$

$$\frac{\langle n_{\bar{\Xi}} \rangle}{\langle n_{\Xi} \rangle} = \lambda_q^{-2} \lambda_s^{-4}; \quad (11.21b)$$

$$\frac{\langle n_{\bar{\Omega}} \rangle}{\langle n_{\Omega} \rangle} = \lambda_s^{-6}; \quad (11.21c)$$

$$\frac{\langle n_{K^+} \rangle}{\langle n_{K^-} \rangle} = \lambda_s^{-2} \lambda_q^2; \quad (11.21d)$$

$$\frac{\langle n_K \rangle}{\langle n_{\Lambda} \rangle} = \lambda_s^{-2} \lambda_q^{-1} \gamma_q^{-1} \frac{F_K}{F_{\Lambda}}. \quad (11.21e)$$

In a more colloquial notation found also in this book, one omits  $\langle n \rangle$ , using as the symbol for the particle considered the subscript only.

The baryochemical potential, or more simply, the quark fugacity  $\lambda_q$ , can be deduced from the above stated ratios. Best for this purpose is to consider the ratios not involving quark-pair fugacities  $\gamma_q$  and  $\gamma_s$ . Any two ratios containing only  $\lambda_q$  and  $\lambda_s$  can be combined to evaluate these quantities. Since many more than two ratios are available, a check of the procedure is possible. This, in fact, constitutes a strong confirmation of the validity of phase-space characterization of particle yields. Postponing detailed discussion to chapter 19, we note that all groups that applied this method to study the chemical properties have found extremely good consistency. This implies that the production of particles as different as kaons  $K$  and antiscascades  $\bar{\Xi}$  occurs by a similar mechanism, and nearly at the same instance in the evolution of the fireball; these particles know of each other, either due to processes of rescattering in the HG phase, or simply because they have been produced directly with yields corresponding to the relative size of the phase space.

An example of the consistency relation can be obtained by combining the ratios of cascades, lambdas, and kaons,

$$\frac{\bar{\Xi}/\Xi}{\bar{\Lambda}/\Lambda} = \frac{K^+}{K^-}, \quad (11.22)$$

which is very well satisfied in all measurements of which we are aware. It is important to note that Eq. (11.22) applies a full  $4\pi$  yield. For the central-rapidity particle yield ratio, a correction containing the influence of the velocity of expansion of the fireball has to be applied.

Although the proper determination of the chemical properties is best achieved in a global fit of hadron yields, it is important that we see how the physics of this determination works. It can be seen that the multitude of strange hadrons allows us to determine the value of  $\lambda_s$  in many different ways, for example,

$$\frac{\bar{\Lambda}/\Lambda}{(\bar{\Xi}/\Xi)^2} = \lambda_s^6 \quad (11.23)$$

and similarly

$$\frac{\bar{\Xi}/\Xi}{(\bar{\Lambda}/\Lambda)^2} = \lambda_q^6. \quad (11.24)$$

This estimate produces an answer for the value of these parameters that very accurately agrees with results of global fits.

It is equally easy to fix the ratio  $\gamma_s/\gamma_q$  since comparison of hyperons of unequal strangeness content always yields this pair fugacity ratio. The difficulty is that we have to understand the ratio of phase spaces of the various baryons, which is controlled by the temperature, when we consider the full yield. A first estimate is obtained by comparing in the same  $m_\perp$  range, e.g.,  $\Lambda$  and  $\Xi$ . How this is done is shown in Fig. 8.8 on page 150. Even then, the feed from higher resonances is important and temperature remains an input into the determination of  $\gamma_i$ .

### 11.5 The grand-canonical conservation of strangeness

Using the partition function Eq. (11.19), we can calculate the net strangeness by evaluating

$$\langle N_s \rangle - \langle N_{\bar{s}} \rangle = \lambda_s \frac{\partial}{\partial \lambda_s} \ln \mathcal{Z}_s^{\text{HG}}. \quad (11.25)$$

We find

$$\langle n_s \rangle - \langle n_{\bar{s}} \rangle = \frac{T^3}{2\pi^2} \left[ (\lambda_s \lambda_q^{-1} - \lambda_s^{-1} \lambda_q) \gamma_s \gamma_q F_K \right]$$

$$\begin{aligned}
 &+ (\lambda_s \lambda_q^2 - \lambda_s^{-1} \lambda_q^{-2}) \gamma_s \gamma_q^2 F_Y \\
 &+ 2(\lambda_s^2 \lambda_q - \lambda_s^{-2} \lambda_q^{-1}) \gamma_s^2 \gamma_q F_{\Xi} \\
 &+ 3(\lambda_s^3 - \lambda_s^{-3}) \gamma_s^3 F_{\Omega} \Big]. \tag{11.26}
 \end{aligned}$$

In general, Eq. (11.25) must be equal to zero since strangeness is a conserved quantum number with respect to the strong interactions, and no strangeness is brought into the reaction. The possible exception is dynamic evolution with asymmetric emission of strange and antistrange hadrons. The grand-canonical condition,

$$\langle n_s \rangle - \langle n_{\bar{s}} \rangle = 0, \tag{11.27}$$

introduces an important constraint, i.e., it fixes  $\lambda_s$  in terms of  $\lambda_b$  (and charge  $\lambda_Q$  when the later is considered).

Equation (11.25) can be solved analytically when the contribution of multistrange particles is small:

$$\lambda_s|_0 = \lambda_q \sqrt{\frac{F_K + \gamma_q \lambda_q^{-3} F_Y}{F_K + \gamma_q \lambda_q^3 F_Y}}. \tag{11.28}$$

This relation between the strange chemical potential  $\mu_s|_0 = T \ln \lambda_s|_0$  and the baryochemical potential  $\mu_b = 3T \ln \lambda_q$  is shown for  $\gamma_q = \gamma_s = 1$  in Fig. 11.4. To understand Fig. 11.4, we note that the term with  $\lambda_q^{-3} = e^{-\mu_b/T}$  in Eq. (11.28) will tend to zero as  $\mu_b$  gets larger and the term with  $\lambda_b$  will dominate in denominator. Thus,  $\lambda_s \propto \lambda_b^{-2/3}$ , i.e.,  $\mu_s \propto -\frac{2}{3}\mu_b$  for large  $\mu_b$ . At small  $\mu_b$ , in particular, for relatively small temperatures, the hyperon contribution is small and we see  $\mu_s \propto \frac{1}{3}\mu_b$ . Putting it differently, Eq. (11.28) knows that, in a baryon-rich HG phase,  $q\bar{s}$  ( $K^+, K_0$ ) kaons are the dominant carriers of  $\bar{s}$  quarks, whereas  $qqs$  ( $\Lambda, \Sigma$ ) hyperon states are the main carriers of  $s$  quarks at finite baryon density. We see that the competition between strangeness content in the four classes of strangeness carriers determines, at each temperature  $T$ , the location where one obtains a nontrivial  $\mu_s = 0$  at finite  $\mu_b$ , and the QGP property  $\lambda_s = 1$  is accidentally present in the HG phase. There is no such nontrivial solution at sufficiently high temperature. For  $T > 200$  MeV and  $\gamma_q = \gamma_s = 1$ , only negative strangeness chemical potential is seen in Fig. 11.4.

The line in the  $(\mu_b-T)$  plane corresponding to  $\mu_s = 0$  is the divide between positive and negative values of the strangeness chemical potential in a strangeness-balanced hadronic gas. The relation between  $\mu_b$  and  $T$  corresponding to  $\mu_s = 0$ , i.e.,  $\lambda_s = 1$ , arising from Eq. (11.26) when net strangeness vanishes, can be solved analytically allowing for the effect of multistrange baryons and antibaryons. First, we note that for  $\lambda_s = 1$ ,

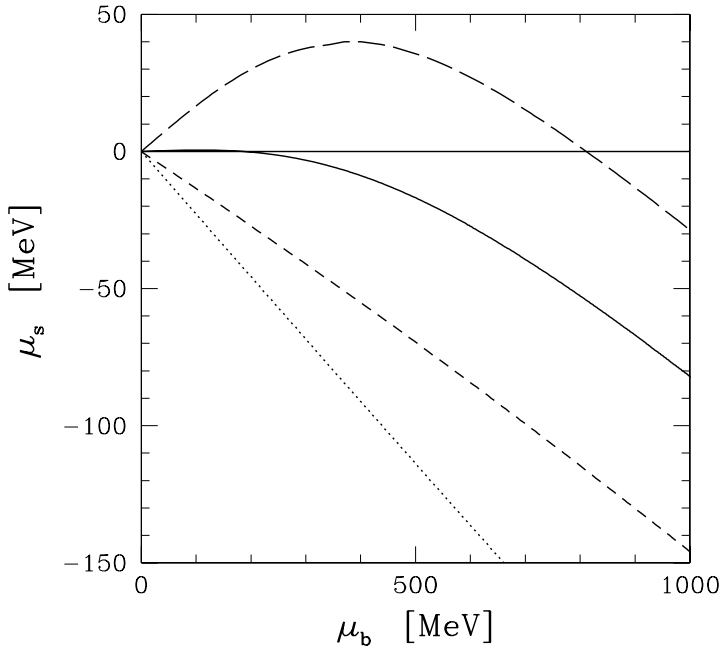


Fig. 11.4. The strange-quark chemical potential  $\mu_s$  versus the baryon chemical potential  $\mu_b$  in a strangeness-neutral grand-canonical chemically equilibrated HG. The long-dashed line corresponds to  $T = 150$  MeV, the solid line to  $T = 200$  MeV, and the short-dashed line to  $T = 300$  MeV. The dotted line is the limiting curve for large  $T$ , computed here at  $T = 1000$  MeV.

there is always an exact balance between  $\Omega$  and  $\bar{\Omega}$  and this term disappears. The coefficient of the hyperon  $F_Y$  contribution, when it is written in the form

$$\lambda_q^{-2} - \lambda_q^2 = (\lambda_q^{-1} - \lambda_q) (\lambda_q^{-1} + \lambda_q),$$

allows us to cancel out a common factor  $\lambda_q^{-1} - \lambda_q$  present in all terms, along with  $\gamma_q \gamma_s$ . We obtain

$$\mu_b = 3T \ln(x + \sqrt{x^2 - 1}), \quad 1 \leq x = \frac{F_K - 2\gamma_s F_{\Xi}}{2\gamma_q F_Y}. \quad (11.29)$$

This result is shown in Fig. 11.5. We have chosen to consider the nonequilibrium condition  $\gamma_q = e^{m_\pi/(2T)}$  corresponding to the maximum entropy content in a hadronic gas, as could be emerging from hadronization of an entropy-rich QGP phase. The solid line is for  $\gamma_s = \gamma_q$ , while the dashed lines span the range  $\gamma_s = 0.8$ – $2.8$  in steps of  $0.2$ , from right to left.

Below and to the left of this separation line in Fig. 11.5, we have positive strangeness chemical potential in a strangeness-balanced HG phase,

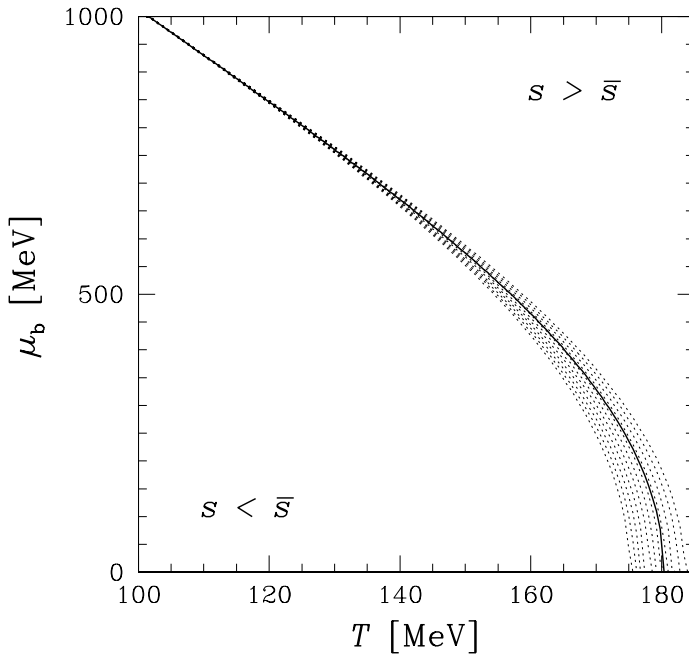


Fig. 11.5. The condition of vanishing strangeness at  $\lambda_s = 1$  in a hadronic gas, evaluated for its maximum entropy content, i.e., with  $\gamma_q = e^{m_\pi/(2T)}$ . Solid line,  $\gamma_s = \gamma_q$ ; dashed lines from left to right are for  $\gamma_s = 0.8$ – $2.8$  in steps of  $0.2$ .

whereas above and to the right we have negative strangeness potential. The importance of this observation is that the relative yield  $R_\Omega \equiv \Omega/\bar{\Omega}$ , Eq. (11.21c), is strongly sensitive to the sign of  $\mu_s$ . At present, we know that, at the SPS top energy, both in S–W and in Pb–Pb interactions,  $R_\Omega \geq 1$  and thus  $\lambda_s \geq 1$  and  $\mu_s \geq 0$ ; the allowed range of  $T$ – $\mu_b$  is below and to the left in Fig. 11.5. Indeed, all analyses of the abundances of particles of which we are aware have yielded results in this domain of  $T$  and  $\mu_b$ .

We further denote, in Fig. 11.5, the area below and to the left as  $s < \bar{s}$ , whereas the domain above and to the right is denoted as  $s > \bar{s}$ . What we indicate is that, for  $\lambda_s = 1$ , the resulting phase space of strange particles would add up to satisfy these conditions within these domains of  $T$  and  $\mu_b$ . To recognize the importance of this condition consider that a QGP is evaporating hadrons. Below and to the left, with  $s < \bar{s}$ , the evaporation favors emission of antistrangeness and this allows the accumulation of an excess of strangeness in the evaporation remnant; this is the process called ‘strangeness distillation’ [134, 135].

The result of the distillation is the production of strangelets, drops of quark matter with an unusually high abundance of  $s$  quarks. Since strange quarks are negatively charged, such states would have unusually small charge relative to their mass; indeed in the limit of equal abundance of  $u$ ,  $d$ , and  $s$ , a strangelet would be neutral. Many searches for long-lived (on the scale of strong interactions) strangelets have been performed, without success [44, 45, 232], suggesting that such states are not stable with respect to strong interactions. If they are produced, strangelets are dissociating into strange hadrons rather rapidly. One will note that, in the decay of hadronic strangelets, production of multistrange baryons, and in particular  $\Omega$ , would be well above the normal expectations. Since the statistical yield of  $\Omega$  is very small, even a small yield of strangelets could lead to visible distortions of the otherwise rarely produced  $\Omega$ . An excess of  $\Omega$  over the statistical-model expectations is seen at the top energy of the SPS; see section 19.3 and Fig. 8.11.

### 11.6 Exact conservation of flavor quantum numbers

We now consider, in more detail, what effect the exact conservation of quantum numbers, such as strangeness or baryon number, has on the size of the available particle phase space. As is intuitively clear, only when the yield numbers are small, can this lead to a noticeable effect. In the grand-canonical approach, flavor conservation, expressed by Eq. (11.27), is not exact. In other words, strangeness, even baryon number, is conserved on average but not exactly. We will focus our interest on the case of newly-produced flavors (strangeness and charm) since the number of pairs of quarks produced can be sufficiently small to warrant this. The exact conservation of the baryon number (or the light-quark flavors) is of particular interest in the study of the small collision systems.

When the number of strange-quark pairs is relatively small, Eq. (11.27) has to be replaced by the sharper ‘canonical’ conservation condition,

$$\langle n_s - n_{\bar{s}} \rangle = 0. \quad (11.30)$$

According to Eq. (11.30), the net strangeness vanishes exactly in each physical system we study. This introduces a correlation between the phase space of particles and of antiparticles and thus, in general, the chemical equilibrium yield of, e.g., the pairs of strange quarks evaluated under constraint Eq. (11.30), is smaller when compared with that expected when Eq. (11.27) is considered.

We are, in particular, interested in understanding under which conditions the canonical and grand-canonical yields are equal, and how the grand-canonical yields are altered by the physical constraint Eq. (11.30) [218]. For strangeness, this amounts to finding the yield for which we can

study the colliding system as if it had infinite size. In the context of the production of charm, the yields (almost) always remain relatively small, and use of the canonical formulation is necessary in order to evaluate the expected chemical-equilibrium yields, even when the grand-canonical approach applies for all the other observables.

The grand partition function, Eq. (10.48), in the Boltzmann limit, can be written as a power series:

$$\mathcal{Z}_{\text{cl}} = e^{Z_f^{(1)}} = \sum_{n=0}^{\infty} \frac{1}{n!} \left( Z_f^{(1)} \right)^n. \tag{11.31}$$

To emphasize that any flavor (in particular s, c, and b) is under consideration here, we generalize slightly the notation  $s \rightarrow f$ . The flavor and antiflavor terms within  $Z_f^{(1)}$  are additive, and we consider at first only singly flavored particles in Eq. (11.19), adopting a simplified and self-explanatory notation:

$$Z_f^{(1)} = \gamma(\lambda_f \tilde{F}_f + \lambda_f^{-1} \tilde{F}_{\bar{f}}), \quad \tilde{F}_i = \frac{VT^3}{2\pi^2} F_i. \tag{11.32}$$

Combining Eq. (11.32) with Eq. (11.31), we obtain

$$\mathcal{Z}_{\text{cl}} = \sum_{n,k=0}^{\infty} \frac{\gamma^{n+k}}{n!k!} \lambda_f^{n-k} \tilde{F}_f^n \tilde{F}_{\bar{f}}^k. \tag{11.33}$$

When  $n \neq k$ , the sum in Eq. (11.33) contains contributions with unequal numbers of f and  $\bar{f}$  terms. Only when  $n = k$  do we have contributions with exactly equal number of f and  $\bar{f}$  terms. We recognize that only  $n = k$  terms contribute to the canonical partition function:

$$Z_{\text{cl}}^{f=0} = \sum_{n=0}^{\infty} \frac{\gamma^{2n}}{n!n!} (\tilde{F}_f \tilde{F}_{\bar{f}})^n = I_0 \left( 2\gamma \sqrt{\tilde{F}_f \tilde{F}_{\bar{f}}} \right). \tag{11.34}$$

The modified Bessel function  $I_0$  is well known, see Eqs. (8.23) and (8.27).

The argument of  $I_0$  has a physical meaning, it is the yield of flavor pairs  $N_{\text{pair}}^{\text{GC}}$  in the grand-canonical ensemble, evaluated with grand-canonical conservation of flavor, Eq. (11.27). To see this, we evaluate

$$\langle N_f \rangle - \langle N_{\bar{f}} \rangle = \lambda_f \frac{\partial}{\partial \lambda_f} \ln \mathcal{Z}_{\text{cl}}^f = \gamma(\lambda_f \tilde{F}_f - \lambda_f^{-1} \tilde{F}_{\bar{f}}) = 0. \tag{11.35}$$

We obtain, see Eq. (11.28),

$$\lambda_f|_0 = \sqrt{\tilde{F}_{\bar{f}}/\tilde{F}_f}, \tag{11.36}$$

and thus

$$\ln \mathcal{Z}_{\text{cl}}^f \Big|_{\lambda_f = \lambda_f|_0} = \langle N_f \rangle + \langle N_{\bar{f}} \rangle = 2\gamma \sqrt{\tilde{F}_f \tilde{F}_{\bar{f}}} \equiv 2N_{\text{pair}}^{\text{GC}}, \tag{11.37}$$

which is just the argument of the  $I_0$  function in Eq. (11.34). In the grand-canonical-ensemble approach the (average) number of pairs  $N_{\text{pair}}^{\text{GC}}$  is extensive in volume, since  $\tilde{F}_i \propto V$ .

In order to evaluate, using Eq. (11.34), the number of flavor pairs in the canonical-ensemble, we need to average the number  $n$  over all the contributions to the sum in Eq. (11.34). To obtain the extra factor  $n$ , we perform the differentiation with respect to  $\gamma^2$  and obtain the canonical ensemble f-pair yield,

$$\begin{aligned} \langle N_f^{\text{CE}} \rangle &\equiv \gamma^2 \frac{d}{d\gamma^2} \ln Z_{\text{cl}}^{f=0} = \gamma \sqrt{\tilde{F}_f \tilde{F}_{\bar{f}}} \frac{I_1 \left( 2\gamma \sqrt{\tilde{F}_f \tilde{F}_{\bar{f}}} \right)}{I_0 \left( 2\gamma \sqrt{\tilde{F}_f \tilde{F}_{\bar{f}}} \right)} \\ &= N_{\text{pair}}^{\text{GC}} \frac{I_1(2N_{\text{pair}}^{\text{GC}})}{I_0(2N_{\text{pair}}^{\text{GC}})}. \end{aligned} \tag{11.38}$$

where we have used Eq. (8.24). The first term is identical to the result we obtained in the grand-canonical formulation, Eq. (11.37). The second term is the effect of exact conservation of flavor.

The intuitive derivation of the canonical constraint we have presented follows the approach of [218]. This can be generalized to more complex systems using the projection method [229, 262]. This method can be applied to solve more complex situations, for example inclusion of multistrange hadrons, conservation of several ‘Abelian’ quantum numbers [61, 102] (such as strangeness, baryon number, and electrical charge), and the problem of particular relevance in this field, the exact conservation of color: all hadronic states, including QGP, must be exactly color ‘neutral’ [111, 112]. The solution of this ‘nonabelian-charge’ problem is most interesting but reaches well beyond the scope of this book.

For the case of ‘Abelian’ quantum numbers, e.g., flavor or baryon number, the projection method arises from the general relation between the grand-canonical and canonical partition functions implicit in Eq. (4.20):

$$\mathcal{Z}(\beta, \lambda, V)_{\text{cl}} = \sum_{n_f = -\infty}^{\infty} \lambda^{n_f} Z_f(\beta, V; n_f). \tag{11.39}$$

In the canonical partition function  $Z_f$ , some discrete (flavor, baryon) quantum number has the value  $n_f \equiv f$ . The inverse of this expansion

is given in Eq. (4.21). On making the substitution  $\lambda = e^{i\varphi}$  we obtain

$$Z_f(\beta, V; n_f) = \int_0^{2\pi} \frac{d\varphi}{2\pi} e^{-in_f\varphi} \mathcal{Z}(\beta, \lambda = e^{i\varphi}, V). \tag{11.40}$$

In the case of the Boltzmann limit, and including singly charged particles only, we obtain for the net flavor  $n_f$  from Eq. (11.33)

$$Z_f(\beta, V; n_f) = \sum_{n,k=0}^{\infty} \frac{\gamma^{n+k}}{n!k!} \int_0^{2\pi} \frac{d\varphi}{2\pi} e^{i(n-k-n_f)\varphi} \tilde{F}_f^n \tilde{F}_f^k. \tag{11.41}$$

The integration over  $\varphi$  yields the  $\delta(n - k - n_f)$  function. Replacing  $n = k + n_f$ , we obtain

$$Z_f(\beta, V; n_f) = \sum_{k=0}^{\infty} \frac{\gamma^{2k+n_f}}{k!(k+n_f)!} \tilde{F}_f^{k+n_f} \tilde{F}_f^k. \tag{11.42}$$

The power-series definition of the modified Bessel function  $I_f$  is

$$I_{n_f}(z) = \sum_{k=0}^{\infty} \frac{(z/2)^{2k+n_f}}{k!(k+n_f)!}. \tag{11.43}$$

Thus we obtain

$$Z_f(\beta, V; n_f) = \left( \frac{\tilde{F}_f}{\tilde{F}_f} \right)^{n_f/2} I_{n_f} \left( 2\gamma \sqrt{\tilde{F}_f \tilde{F}_f} \right). \tag{11.44}$$

The case of  $n_f = 0$  which we considered earlier, Eq. (11.34), is reproduced. We note that, for integer  $n_f$ , we have  $I_{n_f} = I_{-n_f}$ , as is also evident in the integral representation Eq. (8.27). We used  $n_f$  as we would count the baryon number, thus, in flavor counting,  $n_f$  counts the flavored quark content, with quarks counted positively and antiquarks negatively. This remark is relevant when the factors  $\tilde{F}_f$  and  $\tilde{F}_f$  contain baryochemical potential.

When the baryon number is treated in the grand-canonical approach, and strangeness in the canonical approach, there is potential for mathematical difficulties. These can usually be avoided by considering the meromorphic expansion of the partition function Eq. (11.39). Inserting the explicit form Eq. (11.32) we obtain

$$\mathcal{Z}_{cl} \simeq e^{\gamma(\lambda_f \tilde{F}_f + \lambda_f^{-1} \tilde{F}_f)} = \sum_{n_f=-\infty}^{\infty} \lambda_f^{n_f} \left( \frac{\tilde{F}_f}{\tilde{F}_f} \right)^{n_f/2} I_{n_f} \left( 2\gamma \sqrt{\tilde{F}_f \tilde{F}_f} \right). \tag{11.45}$$

Multistrange particles can be introduced as additive terms in the exponent in Eq. (11.45). This allows us to evaluate their yields [148]. However,

the canonical partition function is dominated by singly strange particles and we will assume, in the following, that considering only these suffices to obtain the effect of canonical conservation of flavor. In order to find yields of rarely produced particles such as, e.g.,  $\Omega(sss)$ , we show the omega term explicitly:

$$Z_f(\beta, V; n_f = 0) = \int_0^{2\pi} \frac{d\varphi}{2\pi} e^{\tilde{F}_f e^{i\varphi} + \tilde{F}_{\bar{f}} e^{-i\varphi} + \lambda_\Omega e^{3i\varphi} \tilde{F}_\Omega + \dots}. \tag{11.46}$$

The unstated terms in the exponent are the other small abundances of multiflavored particles. The fugacities not associated with strangeness, as well as the yield fugacity  $\gamma_s$ , are incorporated in Eq. (11.46) into the phase-space factors  $\tilde{F}_i$  for simplicity of notation.

The number of  $\Omega$  is obtained by differentiating  $\ln Z_f(\beta, V)$  with respect to  $\lambda_\Omega$ , and subsequently neglecting the subdominant terms in the exponent,

$$\langle n_\Omega \rangle \simeq \frac{\tilde{F}_\Omega}{I_0} \int_0^{2\pi} \frac{d\varphi}{2\pi} e^{3i\varphi} e^{\tilde{F}_f e^{i\varphi} + \tilde{F}_{\bar{f}} e^{-i\varphi}}. \tag{11.47}$$

The result of the integration is easily read off the meromorphic expansion, Eq. (11.45), to be  $Z_f(\beta, V; n_f = -3)$ , Eq. (11.44). This result is easily understood, the three strange quarks in the particle observed are balanced by the background of singly strange particles (kaons and antihyperons),

$$\langle n_\Omega \rangle \simeq \tilde{F}_\Omega \left( \frac{\tilde{F}_f}{\tilde{F}_{\bar{f}}} \right)^{-3/2} \frac{I_3(2N_{\text{pair}}^{\text{GC}})}{I_0(2N_{\text{pair}}^{\text{GC}})}. \tag{11.48}$$

We recall that, according to Eq. (11.36), the middle term is just the fugacity factor  $\lambda_s^3$ . The first two factors in Eq. (11.48) constitute the grand-canonical yield, while the last term is the canonical  $\Omega$ -suppression factor. A full treatment of the canonical suppression of multistrange particle abundances in small volumes has been used to obtain particle yields in elementary interactions [60].

Similarly, one finds that the suppression of  $\Xi$  abundance has the factor  $I_2/I_0$ , whereas, as discussed for the general example of the flavor-pair yield, the yield of single strange particles is suppressed by the factor  $I_1/I_0$ . The yield of all flavored hadrons in the canonical approach (superscript ‘C’) can be written as a function of the yield expected in the grand-canonical approach in the general form

$$\langle s^\kappa \rangle^{\text{C}} = \tilde{F}_\kappa \left( \frac{\tilde{F}_f}{\tilde{F}_{\bar{f}}} \right)^{\kappa/2} \frac{I_{|\kappa|}(2N_{\text{pair}}^{\text{GC}})}{I_0(2N_{\text{pair}}^{\text{GC}})} = \langle s^\kappa \rangle^{\text{GC}} \frac{I_{|\kappa|}(2N_{\text{pair}}^{\text{GC}})}{I_0(2N_{\text{pair}}^{\text{GC}})}, \tag{11.49}$$

with  $\kappa = \pm 3, \pm 2$ , and  $\pm 1$  for  $\Omega, \Xi$ , and Y and K, respectively. On the left-hand side in Eq. (11.49) the power indicates the flavor content in the

particle considered, with negative numbers counting antiquarks. We note, on inspecting the final form of Eq. (11.49), that the canonical suppression of particle and antiparticle abundances is the same, certainly so when we study systems with several pairs present. In very small systems, one may need to evaluate the quantum distributions including multistrange particles in order to obtain precise results. A particle/antiparticle asymmetry can occur if baryon/antibaryon asymmetry applies.

The simplicity of Eq. (11.49) originates from the assumption that the contributions of singly strange particles to conservation of strangeness are dominant. This assumption is consistent with the neglect of quantum statistics. In fact, on expanding the Bose distribution for kaons, one finds that the next-to-leading-order contribution, which behaves as strangeness  $n_s = \pm 2$  hadrons, is dominating the influence of all multistrange hadrons. Our study is consistent with the Boltzmann statistics assumed here; more complex evaluation taking multistrange hadrons into account, but considering kaons as Boltzmann particles, is theoretically inconsistent.

### 11.7 Canonical suppression of strangeness and charm

The canonical flavor yield suppression factor,

$$\eta \equiv \frac{I_1\left(2\gamma\sqrt{\tilde{F}_f\tilde{F}_{\bar{f}}}\right)}{I_0\left(2\gamma\sqrt{\tilde{F}_f\tilde{F}_{\bar{f}}}\right)} = \frac{I_1(2N_{\text{pair}}^{\text{GC}})}{I_0(2N_{\text{pair}}^{\text{GC}})} < 1, \quad (11.50)$$

depends in a complex way on the volume of the system, or, expressing it alternatively, on the grand-canonical number of pairs,  $N_{\text{pair}}^{\text{GC}}$ . The suppression function  $\eta(N) \equiv I_1(2N)/I_0(2N)$  is shown in Fig. 11.6 as a function of  $N$ . For  $N > 1$ , we see (dotted lines) that the approach to the grand-canonical limit is relatively slow; it follows the asymptotic form

$$\eta \simeq 1 - \frac{1}{4N} - \frac{1}{128N^2} + \dots, \quad (11.51)$$

whereas for  $N \ll 1$ , we see a nearly linear rise:

$$\eta = N - \frac{N^3}{2} + \dots. \quad (11.52)$$

Overall, when the the yield of particles is small, we have, using Eq. (11.52),

$$N_{\text{pair}}^{\text{CE}} = (N_f^{\text{GC}})^2. \quad (11.53)$$

Hagedorn was puzzled by this quadratic behavior of the particle yield, being concerned about rarely occurring astrophysical processes of pair production. In his 1970/71 CERN lectures [141], he asked how the yield

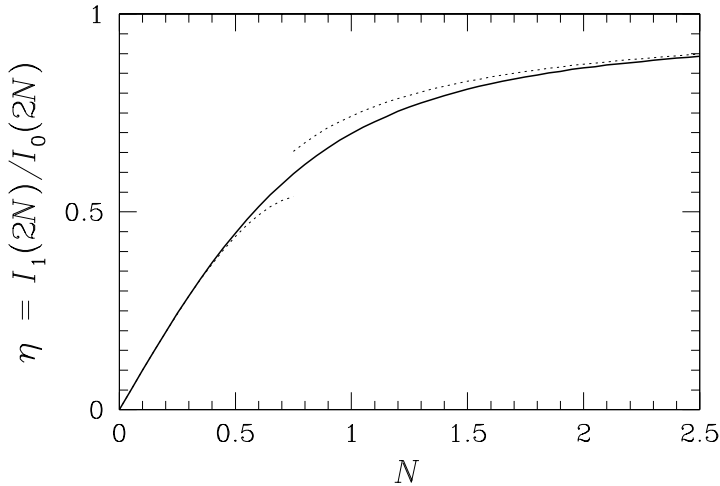


Fig. 11.6. Solid line: the canonical yield-suppression factor as a function of the grand-canonical yield of particles  $N$ . Dotted lines: asymptotic expansion forms presented in the text.

of particles can be  $Y \propto e^{-2m/T}$ , when the threshold for production of a pair is relevant, and another time  $Y \propto e^{-m/T}$ , when the statistical yield is evaluated. This is the grand-canonical yield for  $m > T$ , as seen in section 10.4,

$$N^{\text{GC}} = \frac{g_f}{2\pi^2} T^3 V \sqrt{\frac{\pi m^3}{2T^3}} e^{-m/T}, \tag{11.54}$$

whereas when the yield of particles is small, e.g., when  $m \gg T$ , the canonical result applies:

$$N^{\text{CE}} = \frac{g_f^2}{8\pi^3} T^3 m^3 V^2 e^{-2m/T}. \tag{11.55}$$

We see that the Hagedorn puzzle has been resolved. The reaction volume is an important factor controlling which of the two results Eqs. (11.54) and (11.55) should be considered in a given physical situation.

We next consider whether there is any effect of QGP compared with HG in the study of canonical conservation of strangeness. The possible difference would arise from the different sizes of the phase space for strangeness in these two phases of matter. In the Boltzmann limit, the flavor and antiflavor phase space in the symmetric QGP is:

$$\tilde{F}_f = \tilde{F}_{\bar{f}} = g_f V \int \frac{d^3p}{(2\pi)^3} e^{\frac{\sqrt{p^2+m_f^2}}{T}} = \frac{3VTm_f^2}{\pi^2} K_2(m_f/T). \tag{11.56}$$

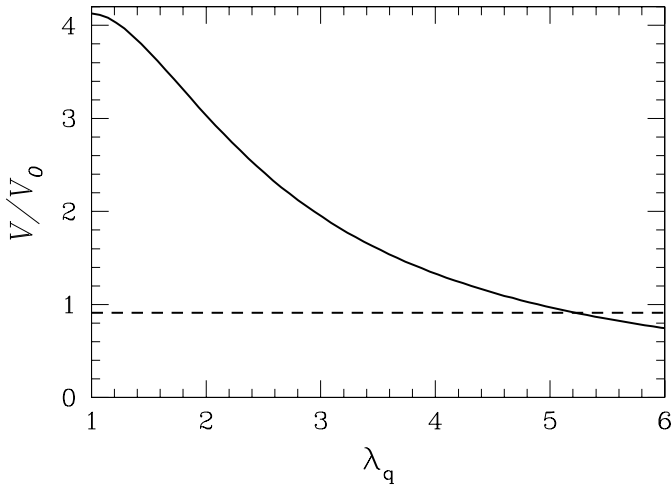


Fig. 11.7. Volume needed for one strange quark pair using grand-canonical counting as function of  $\lambda_q$  for  $T = 160$  MeV,  $\gamma_q = 1$ ,  $\gamma_s = 1$ ,  $V_h = (4\pi/3) 1 \text{ fm}^3$ . Solid line: hadron gas phase space, dashed line: quark phase space with  $m_s = 160$  MeV.

For the hadronic phase, it is derived from Eqs. (11.19) and (11.20). We have, counting strange-quark content as positively ‘flavor charged’ as before,

$$\tilde{F}_f = \lambda_q^{-1} \tilde{F}_K + \lambda_q^2 \tilde{F}_Y, \quad (11.57)$$

$$\tilde{F}_{\bar{f}} = \lambda_q \tilde{F}_K + \lambda_q^{-2} \tilde{F}_Y. \quad (11.58)$$

All these quantities  $\tilde{F}_i$  are proportional to the reaction volume.

The interesting result, seen in Fig. 11.6, is that the suppression of yield is at the level of 30% when one pair of particles would be expected to be present in grand-canonical chemical equilibrium; the suppression means that instead we find that the true phase-space yield is 0.7 pairs. Actually, in p–p interactions at 158 GeV/c projectile momentum, the analysis of experimental results yields  $0.66 \pm 0.07$  strange pairs [277].

Pursuing this line of thought, but also to obtain a reference regarding the magnitudes involved for strangeness, we consider how big a volume we need in order to find (using grand-canonical-ensemble counting) one pair of strange particles. In the hadronic phase space, with  $\lambda_s$  chosen to conserve strangeness, we have

$$\frac{V}{V_h} = \frac{2\pi^2}{V_h T^3 \gamma_q \gamma_s \sqrt{(F_K + \lambda_q^3 F_Y)(F_K + \lambda_q^{-3} F_Y)}}. \quad (11.59)$$

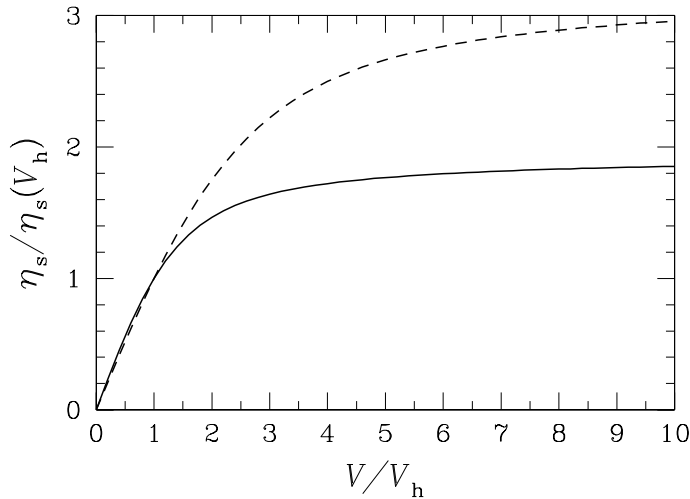


Fig. 11.8. Canonical yield enhancement at large volumes compared with the case of unit hadron volume  $V_h = \frac{4}{3}\pi \text{ fm}^3$ . Solid line, QGP phase; dashed line, HG.

For p–p interactions, we consider  $T = 160 \text{ MeV}$ , and the elementary hadronic volume is chosen to be  $V_h = \frac{4}{3}\pi \text{ fm}^3$ . The applicable value of  $\lambda_q$ , if statistical methods are used, is close to unity. The result is shown as the solid line in Fig. 11.7, as a function of  $\lambda_q$ , for  $\gamma_q = 1$  and  $\gamma_s = 1$ . The dashed line is the corresponding result for the QGP strange-quark phase space, which naturally does not depend on  $\lambda_q$ , and has been obtained by choosing  $m_s = 160 \text{ MeV}$ . Just a little less than one hadronic volume suffices; one finds one pair in  $V_h$  for  $m_s = 200 \text{ MeV}$ .

We show in Fig. 11.8 the canonical strangeness-suppression factor Eq. (11.50), both for a QGP (solid line) and for a HG (dashed line). We have converted the suppression  $\eta$  into an enhancement by normalizing at  $\eta(V = V_h)$ . For the QGP, we take  $m_s = 160 \text{ MeV}$ , whereas, for a HG, we take  $\mu_b = 210 \text{ MeV}$ . Both phases are considered at  $T = 145 \text{ MeV}$ . Since the strangeness content in QGP is greater than that in HG, there is less ‘catching up’ to do and the overall yield is increased by factor 1.8, whereas for HG, we find an increase by a factor of three. Practically all of this enhancement occurs when the reaction volume increases to five, i.e., for rather small reaction systems.

We now look at the suppression of multistrange particle abundances by the factors  $\eta_3(N) = I_3(2N)/I_0(2N)$ , for  $\Omega$ , and  $\eta_2(N) = I_2(2N)/I_0(2N)$ , for  $\Xi$ . For small values of  $N$ , we obtain

$$\eta_\kappa \equiv \frac{I_\kappa(2N)}{I_0(2N)} \rightarrow N^\kappa \frac{1}{\kappa!} \left( 1 - \frac{\kappa}{\kappa + 1} N^2 \right). \tag{11.60}$$

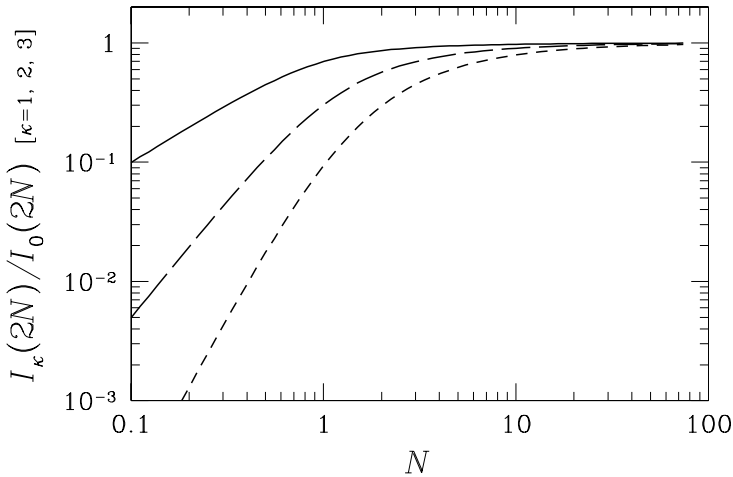


Fig. 11.9. Canonical yield-suppression factors  $I_\kappa/I_0$  as function of the grand-canonical particle yield  $N$ . Short-dashed line: the suppression of triply-flavored hadrons; long-dashed line: the suppression of doubly-flavored hadrons; and solid line, the suppression of singly-flavored hadrons.

This result is easily understood on physical grounds: for example, when the expected grand-canonical yield is three strangeness-containing pairs, it is quite rare that all three strange quarks go into an  $\Omega$ . This is seen in Fig. 11.9 (short-dashed curve), and in fact this will occur about a tenth as often as we would expect from computing the yield of  $\Omega$ , ignoring the canonical conservation of strangeness. The other lines in Fig. 11.9 correspond to the other suppression factors; the long-dashed line is  $\eta_2(N) = I_2(2N)/I_0(2N)$  and the solid line is  $\eta(N) = I_1(2N)/I_0(2N)$ . They are shown to be dependent on the number of strange pairs expected in the grand-canonical equilibrium, denoted in Fig. 11.9 as  $N$ .

It has been proposed to exploit the canonical suppression which grows with strangeness content to explain the increase in production of strange hadrons seen in Fig. 1.6 on page 19, when the per-participant yield in A–A interactions is compared with that from p–Be interactions [228]. A direct comparison of the reduction factors  $\eta_\kappa$  is possible. Choosing as the reference point the yield  $N \lesssim 1$ , the claim is that one can come close to explaining the enhancement in production of three out of five strange hadrons seen in Fig. 1.6. The reader should notice that the enhancement effect is derived from the suppression of the base yield in the small reference system. We obtain this effect by rebasing the results shown in Fig. 11.9 to the strangeness yield observed in p–p reactions evaluated within canonical formulation; see Fig. 11.10. The three cases studied in Fig. 11.9 are seen, where the dotted lines are derived from

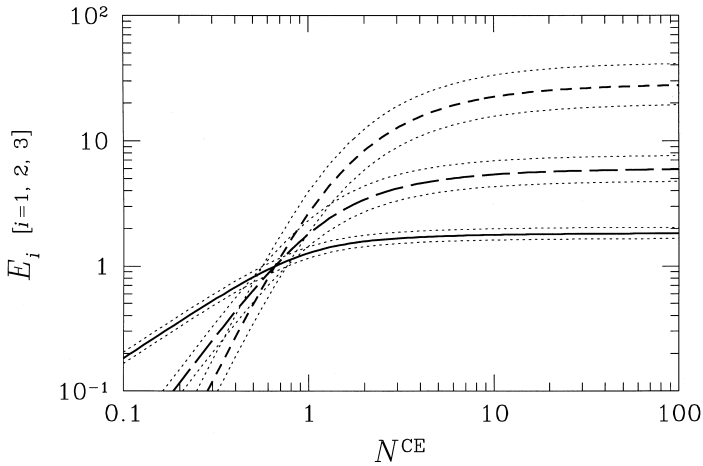


Fig. 11.10. Canonical yield-suppression factor of Fig. 11.9 expressed as enhancement factors  $E_i$ ,  $i = 1, 2, 3$  as functions of the canonical-pair-particle yield  $N^{\text{CE}}$ . Solid line:  $E_1$ , the enhancement of singly-flavored hadrons, relative to the yield  $0.66 \pm 0.07$ , expected in p–p reactions. Similarly, long-dashed line:  $E_2$ , enhancement of doubly-flavored hadrons; and short-dashed line:  $E_3$ , enhancement of triply-flavored hadrons. Dotted lines correspond to the errors arising from the error in the strangeness yield, to which the results are normalized.

the error in the reference yield of production of strangeness in p–p reactions.

We see, in quantitative terms, the strength of the canonical effect, especially for multistrange hadrons, and its rapid rise with the yield of strangeness [223]. The canonical-enhancement effect rises rapidly but smoothly and saturates at the grand-canonical yield in rather small systems. The grand-canonical chemical-equilibrium yield is reached for systems comprising ten strangeness pairs and for reaction systems about six times greater than the p–p system, considering that the yield of singly-strange particles is enhanced by a factor three, as is seen in Fig. 11.10. This result is inconsistent with the experimental results from the NA52 experiment [153], which reveal an abrupt threshold for enhancement of production of strangeness at  $\simeq 50$  participants, just where the WA57 team recently reported a sudden onset of enhancement in yield of  $\Xi^-$  [108]. Given the sensitivity of the results shown in Fig. 11.10 to the strangeness reference yield, it is natural to conclude that the explanation of strange-hadron enhancement offered in [228] is based on a fine tuned p–Be strangeness yield, not cross-checked with the (at-present-unavailable) experimental yield.

We addressed, with such a great precision, the canonical chemical-equilibrium yields of strange particles expected to originate from small

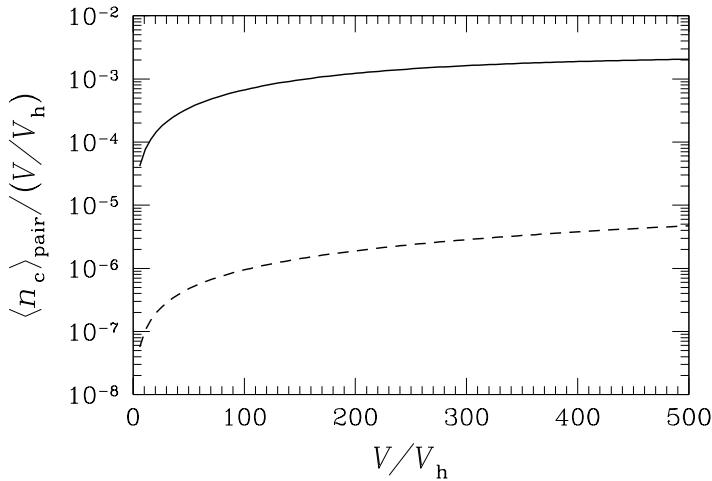


Fig. 11.11. The canonical yield of pairs of open charm quarks  $\langle n_c \rangle_{\text{pair}}$  per unit volume as a function of volume, in units of  $V_h = \frac{4}{3}\pi \text{ fm}^3$ . Solid line, QGP with  $m_c = 1.3 \text{ GeV}$ ; dashed line, HG at  $\mu_b = 210 \text{ MeV}$ , both phases at  $T = 145 \text{ MeV}$ .

systems, since hadron yields observed in p–p and p– $\bar{\text{p}}$  interactions, and even in hadron jets produced in LEP  $e^+e^-$  reactions are remarkably close to the expectations for chemical equilibrium [62], allowing in the analysis for the canonical suppression and including the effects of quantum degeneracy. This thorough analysis results in a not completely satisfactory  $\chi^2$  per degree of freedom (= 61/21). Yet a reader of this thorough report will have the impression that a modern-day Maxwell’s demon must be at work, generating canonical chemical equilibria for hadrons in all these elementary interactions, and abundances of strange quarks within a factor of two of absolute chemical equilibrium.

On the other hand, a demon that works for strangeness should also work for charm. The yield of charm in Pb–Pb interactions is estimated from the lepton background at 0.5 pairs per central collision [13]. We can use the small- $N$  expansion, Eq. (11.60). The corresponding A–A canonical enhancement factor, compared with p–A, is  $N_{AA}/N_{pA} \simeq 100A$ . (Here  $N$  is now the yield of ‘open’ charm rather than strangeness.) The measured open-charm cross sections, however, scale with the number of participants, and there is no space for a large canonical enhancement/suppression of production of charm. To be more specific, we show, in Fig. 11.11, the specific yield of charm  $\langle n_c \rangle_{\text{pair}}$  per unit volume as a function of the volume. The canonical effect is the deviation from a constant value and it is significant,  $\mathcal{O}(100)$ . Even at  $V = 500V_h$  the infinite-volume grand-canonical limit is not yet attained, for the case of the larger phase space of QGP (solid line), the total yield of charm is just one charm pair. The absolute

yield in both phases is strongly dependent on the temperature used, here  $T = 145$  MeV. In QGP, we took  $m_c = 1.3$  GeV. The phase space of a HG includes all known charmed mesons and baryons, with abundances of light quarks controlled by  $\mu_b = 210$  MeV and  $\mu_s = 0$ .

Although, by choosing a slightly higher value of  $T$ , we can easily increase the equilibrium yield of charm in a HG to the QGP level [133], this does not eliminate the effect of canonical suppression of production of charm if chemical equilibrium is assumed for charm in the elementary interactions. We are simply so deep in the ‘quadratic’ domain of the yield, see Eq. (11.60), that playing with parameters changes nothing, since we are constrained in Pb–Pb interactions by experiment to have a yield of charm of less than one pair.

It is natural to argue that the very heavy charm quarks are not in chemical equilibrium, and that their production has to be studied in kinetic theory of collision processes of partons. However, this means that there is no twenty-first-century Maxwell’s demon with control of charm, and, of course, also not of strangeness. The production and enhancement of charm and strangeness in heavy-ion collisions is in our opinion a kinetic phenomenon. To study it, we should explore a wide range of collision volume and energy. The objective is to determine boundaries of the high, possibly QGP-generated, yields.

## 12 Hagedorn gas

### 12.1 The experimental hadronic mass spectrum

One of the most striking features of hadronic interactions, which was discovered by Hagedorn [140], is the growth of the hadronic mass spectrum with the hadron mass. With the 4627 different hadronic states we have used in the study of properties of HG in section 11.1 [136], it is reasonable to evaluate the mass spectrum of hadronic states  $\rho(m)$ , defined as the number of states in the mass interval  $(m, m + dm)$ . We represent each particle by a Gaussian, and obtain  $\rho(m)$  by summing the contributions of individual hadronic particles:

$$\rho(m) = \sum_{m^*=m_\pi, m_\rho, \dots} \frac{g_{m^*}}{\sqrt{2\pi}\sigma_{m^*}} \exp\left(-\frac{(m - m^*)^2}{2\sigma_{m^*}^2}\right). \quad (12.1)$$

Here,  $g_{m^*}$  is the degeneracy of the hadron of mass  $m^*$  including, in particular, spin and isospin degeneracy, and  $\sigma = \Gamma/2$ ,  $\Gamma = \mathcal{O}(200)$  MeV being the width of the resonance. The pion, with  $m_\pi \simeq \sigma$  is a special case, and is set aside in such smoothing of the mass spectrum. Downward modification of its mass has a great impact on properties of HG and is thus not allowed.